Computation of the Mid-Sagittal Plane in 3D Medical Images of the Head

Sylvain Prima, Sébastien Ourselin, Nicholas Ayache

INRIA

INSTITUT NATIONAL DE RECHERCHE EN INFORMATIQUE ET EN AUTOMATIQUE

Computation of the mid-sagittal plane in 3D medical images of the head

Sylvain Prima — Sébastien Ourselin — Nicholas Ayache

N° 3841

Décembre 1999

THÈME 3

ISSN 0249-6399 ISRN INRIA/RR--3841--FR+ENG

INRIA
SOPHIA ANTIPOLIS

Computation of the mid-sagittal plane in 3D medical images of the head

Sylvain Prima , Sébastien Ourselin , Nicholas Ayache

Thème 3 — Interaction homme-machine,
images, données, connaissances
Projet EPIDAURE

Rapport de recherche n° 3841 — Décembre 1999 — 39 pages

Abstract: We present a new symmetry-based method allowing to compute, reorient and recenter the mid-sagittal plane in anatomical and functional 3D images of the brain. In the literature, there are mainly two definitions of this plane: it is either the plane best fitting the inter-hemispheric fissure of the brain, or the plane best superposing the two sides of the head by reflective symmetry. We use this latter definition in our method, which is composed of two steps. At first, the computation of local similarity measures between the two sides of the brain allows to match homologous anatomical structures or functional areas, by way of a block matching procedure. The output is a set of point-to-point correspondences: the centers of homologous blocks. Subsequently, we define the mid-sagittal plane as the one superposing at best the points in one side of the head and their counterparts in the other side by reflective symmetry. The estimation of the parameters characterizing the plane is performed by a least trimmed squares optimization scheme. Then, the estimated plane is aligned with the center of the image lattice. This method is fully automated, objective and reproducible.

Our method tackles the main issue posed by the symmetry-based approach, that often relies on global similarity measures (such as the cross-correlation) between the intensities of the two flipped versions of the 3D image. The estimation of the mid-sagittal plane can be severely biased when normal or abnormal

Unité de recherche INRIA Sophia Antipolis
2004, route des Lucioles, B.P. 93, 06902 Sophia Antipolis Cedex (France)
Téléphone : 04 92 38 77 77 - International : +33 4 92 38 77 77 —Fax : 04 92 38 77 65 - International : +33 4 92 38 77 65

asymmetries hide the underlying symmetry of the brain or the skull. The computation of local measures of symmetry and the use of a robust estimation technique allow to discriminate between symmetrical and asymmetrical areas. Then, the mid-sagittal plane is mainly computed from the underlying gross symmetry of the brain, because its estimation is robust with respect to normal or abnormal asymmetries which are treated as outliers. We show on a large database of synthetic images that we can obtain a subvoxel accuracy in a CPU time of about 3 minutes, for strongly tilted heads, noisy and biased images. We present results on isotropic or anisotropic anatomical (MR, CT), and functional (SPECT and PET) images.

Key-words: medical image analysis, brain, skull, symmetry, inter-hemispheric fissure, mid-sagittal plane, block matching, robust estimation, least trimmed squares.

Calcul du plan médian sagittal dans les images médicales 3D du cerveau

Résumé : Nous présentons une nouvelle méthode pour calculer, réorienter et recentrer le plan médian sagittal du cerveau dans les images médicales tridimensionnelles du cerveau. Deux définitions différentes de ce plan sont généralement utilisées dans la littérature : il s'agit soit du plan passant au mieux le long de la fissure inter-hémisphérique, soit du plan superposant au mieux les deux hémisphères du cerveau par réflexion. Notre méthode, reposant sur cette dernière définition, se décompose en deux étapes. Dans un premier temps, le calcul de mesures de similarité locales entre les deux hémisphères du cerveau nous permet de mettre en correspondance les zones anatomiquement ou fonctionnellement homologues, par le biais d'un algorithme d'appariement de blocs cubiques de voxels. Nous définissons le plan médian sagittal comme celui superposant au mieux les centres des blocs définis dans un hémisphère avec les centres de leurs correspondants dans l'autre hémisphère. L'estimation des paramètres de ce plan est effectuée de façon robuste par la méthode des moindres carrés triés (least trimmed squares). Enfin, ce plan est automatiquement aligné avec le centre de l'image.

Notre méthode, objective et reproductible, permet de traiter le problème majeur posé par les approches fondées sur des critères de symétrie, qui reposent souvent sur la maximisation d'un critère de similarité global. Dans ce cas, l'estimation du plan peut être fortement faussée par la présence de régions dissymétriques ou asymétriques, qui masquent la symétrie sous-jacente du cerveau. Le calcul de mesures de similarité locales et l'utilisation d'une technique d'estimation robuste permet de discriminer les zones symétriques des autres. Ainsi, le calcul du plan qui en résulte est essentiellement fondé sur les zones fortement symétriques. Nous validons notre méthode sur une large base de données synthétiques, et montrons que nous pouvons atteindre une précision inférieure à la taille des voxels en un temps CPU de 3 minutes environ, pour des cerveaux fortement décentrés et des images fortement bruitées et biaisées. Nous présentons des résultats sur des images réelles isotropes ou non, anatomiques (résonance magnétique, scanner X) ou fonctionnelles (TEP, TESP).

Mots-clés : analyse des images médicales, cerveau, crâne, symétrie, fissure inter-hemisphérique, plan médian sagittal, appariement de blocs, estimation robuste, moindres carrés triés.

1 Introduction

1.1 Presentation of the problem

A normal human head exhibits a rough bilateral symmetry. What is easily observable for external structures (ears, eyes, nose, skull...) remains valuable for the brain and its components. It is split into two hemispheres, in which each substructure has a counterpart of approximately the same shape and location in the opposite side (temporal, frontal, occipital lobes, ventricles...). The hemispheres are connected to each other by the corpus callosum, and separated by a grossly planar, mid-sagittal, fissure.

However, it has been reported since the late 19th century that conspicuous morphological differences between the hemispheres make the brain systematically asymmetrical. For example, the wider right frontal and left occipital lobes give rise to a torque effect of the overall brain shape (see Figure 1). More subtly, the natural variability of the cortex translates into slight differences between hemispheres. In the same way, cerebral dominance has been demonstrated since the work of Paul Broca on the language lateralization (1861), and many brain functions are now thought or known to be located in mainly one of the hemispheres (handedness, visual abilities, etc.). The question of whether the anatomical and the functional brain asymmetries relate to each other remains debatable to the point, even if evidences of close connections have been demonstrated quite lately [6]. These studies suggest that symmetry considerations are key to the understanding of cerebral functioning.

Volumetric medical images convey information about anatomical (MR, CT) or functional (PET, SPECT) symmetries and asymmetries, but they are often blurred by acquisition artifacts (noise, bias), and above all by the usual tilt of the patient's head in the device during the scanning process. More precisely, the "ideal" coordinate system attached to the head, in which the inter-hemispheric fissure is conveniently displayed, differs from the coordinate system of the image by three angles around the bottom-top (yaw angle, axial rotation), the back-front (roll angle, coronal rotation) and the left-right (pitch angle, sagittal rotation) axes, and three translations along these directions (see Figure 2). It means that the fissure is generally not displayed in the center of the image lattice. This prevents from further visual inspection or analy-

sis, because the homologous anatomical structures or functional areas in both hemispheres are not displayed in the same axial or coronal slice in the 3D image.

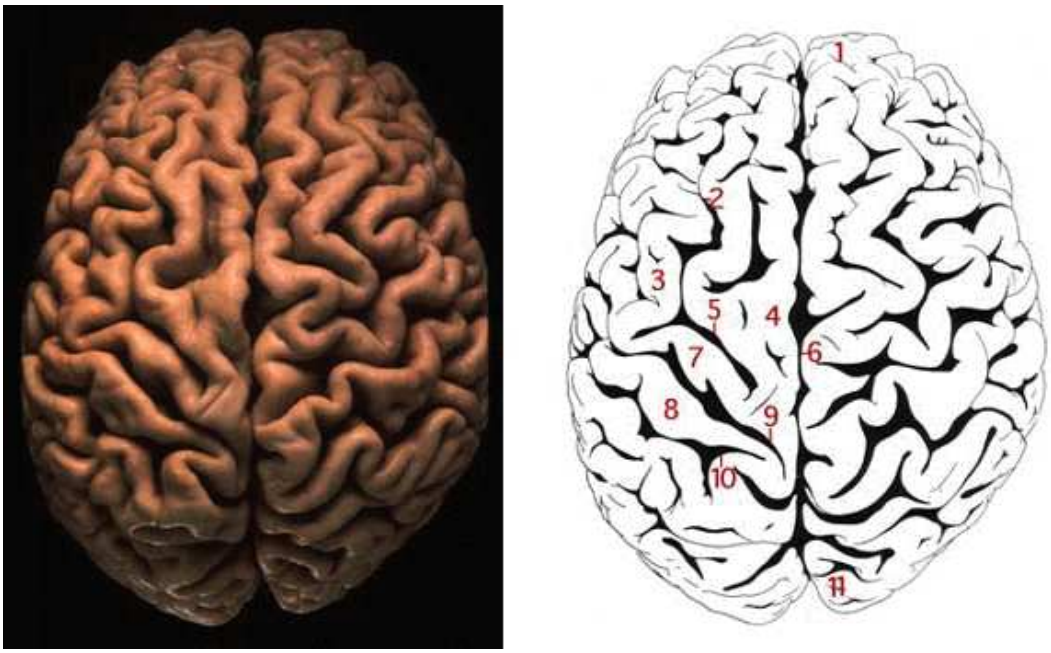

Figure 1: Torque effect of the brain: the right frontal lobe (1) is larger than the left one, and this is the opposite for the occipital lobe (11). Description of the hemispheres: 1. Frontal pole 2. Superior frontal sulcus 3. Middle frontal gyrus 4. Superior frontal gyrus 5. Precentral sulcus 6. Longitudinal cerebral fissure 7. Precentral gyrus 8. Postcentral gyrus 9. Central sulcus 10. Postcentral sulcus 11. Occipital pole. This illustration comes from the Virtual Hospital [27].

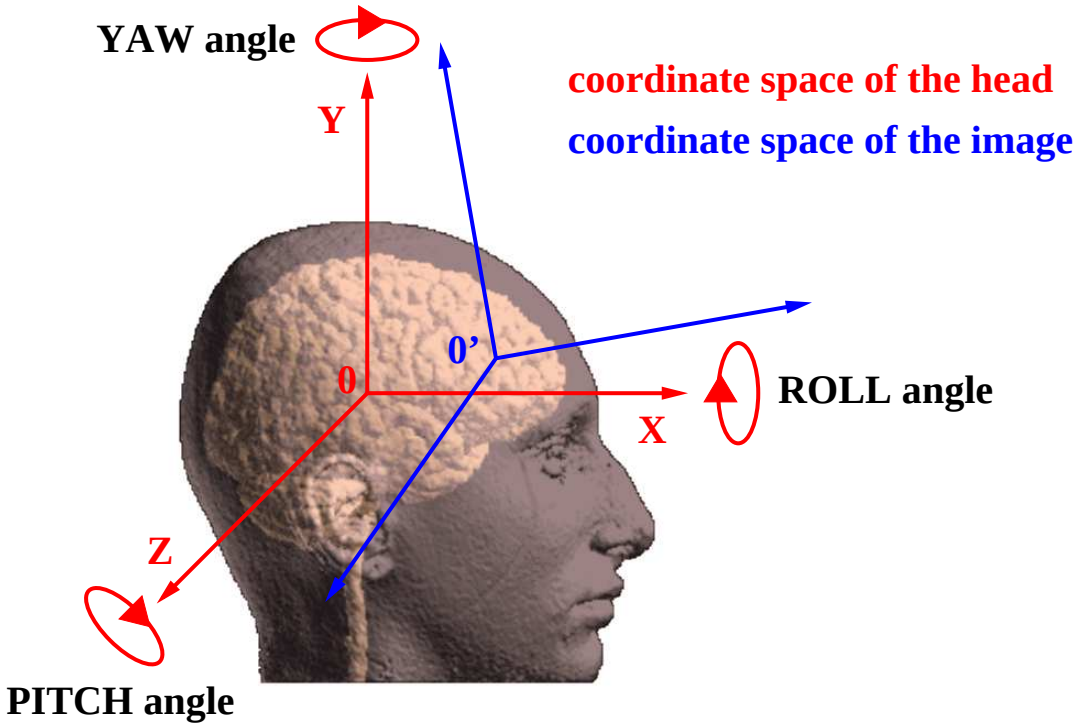

Figure 2: The "ideal" coordinate system attached to the head (in which the fissure is close to the plane $Z = 0$) and the coordinate system of the image are deduced to each other by way of three angles (yaw, roll and pitch) and a 3D translation $(\overrightarrow{OO'})$.

Thus, it is often of great interest to correctly reorient and recenter head images, because normal (torque effect, intrinsic variability, ...) and abnormal (unilateral pathologies) departures from symmetry appear more clearly. This can be helpful for detection and diagnosis in many cases: fractures of the skull in CT images, lesions, or bleed in MR images, asymmetries of perfusion in SPECT images, etc. Some diseases are assumed to be strongly linked with abnormalities of brain asymmetry, like schizophrenia: in this case, the brain is suspected to be more symmetrical than normal [4].

After the initial tilt has been corrected, it is easier to perform further manual or automatic measurements to compare the two sides of the brain. In [7], the distances between the external surface of the hemispheres and the mid-sagittal plane of the reoriented, recentered image are computed; these measures provide a quantitative 2D symmetry map. In [23, 14, 24], a dense 3D field is computed over the whole brain, between the head and its symmetric with respect to the mid-sagittal plane of the image. This field translates the brain symmetry; in particular, it is null where the brain is perfectly symmetrical. More generally, brain analysis often requires the computation of volume ratios between left and right, which is easier when their relative location is immediate to assess. At last, it must be noted that it is often a useful preprocessing step in MR images for higher level tasks such as putting the data in a stereotaxic coordinate system [21].

Several papers have previously considered the problem of correcting the axial and coronal rotations, and the translation along the left-right axis; we give a brief overview of the state-of-the-art in the next section. Note that the correction of the sagittal rotation (e.g., the alignment along the AC-PC line) and the translations along the bottom-top and the back-front axes is a very different problem that we won't tackle here.

1.2 Existing methods

Most of the existing algorithms share a common methodology. First, a proper mid-sagittal plane is defined in the head, generally different from the mid-sagittal plane of the image, because of the tilt. Then the head is rotated and centered straightforwardly, so that the extracted plane matches the center of the image lattice. There are mainly two classes of methods, differing in their

definition of the searched plane, which can be either the plane best matching the inter-hemispheric fissure or the plane maximizing a symmetry criterion, i.e., making the 2 parts of the head lying on each side most similar. We detail the advantages and drawbacks of these two approaches in the following, and summarize the main features of the related algorithms in Table 1, at the end of the section.

1.2.1 Methods based on the inter-hemispheric fissure

Hypotheses. The basic hypothesis underlying these methods is that the inter-hemispheric fissure is roughly planar, and that it provides a good landmark for further volumetric symmetry analysis.

Methods. Generally, the fissure is segmented in MR images. In [7, 11], the fissure is extracted slice-by-slice using snakes. Then, a 3D plane is found, using an orthogonal regression from a set of control points representing the segmented curve. In [3], the author proposes a 3D extension of the Hough transform principle to detect the mid-sagittal plane. A Hough transform is computed on each 2D coronal slice to detect straight lines. The accumulator cells of the transform contain the magnitude of the gradient computed in 3D. After these 2D lines are extracted, simple geometrical considerations show how to robustly compute the 3D plane from these lines. As a preprocessing, the head must be segmented to avoid detecting meaningless lines.

Advantages & drawbacks. The main advantage of this approach is that the resulting reorientation and recentering of the brain is insensitive to strong asymmetries, provided there is not a mass effect near the fissure, which is known to be quite stable. As they do not take into account the global symmetry of the whole brain, the counterpart is the sensitivity of these algorithms to the often observed curvature of the fissure (see Figure 1). For example, in [7], the method only relies on a few points representing the snakes, and the orthogonal regression is known not to be robust with respect to outliers: the intrinsic curvature of the fissure and the potential errors of segmentation can strongly corrupt the result. In addition, the Hough transform principle [3] will fail to detect lines if the hypothesis of weak curvature is violated. At last, these methods are not adaptable to other modalities, where the fissure is not clearly visible.

1.2.2 Methods based on a symmetry criterion

Hypotheses. There are relatively simple methods of finding a plane of reflective symmetry in case of perfectly symmetrical geometrical objects, in 2D or 3D. In this case, it can be demonstrated that any symmetry plane of a body is perpendicular to a principal axis. In case of medical images, the problem is slightly different, because normal and abnormal asymmetries hide the underlying symmetry of the head: a perfect symmetry plane does not exist. To tackle this problem, an intuitive idea is to define the mid-sagittal plane as the one that maximizes the similarity between the image and its symmetric, i.e., the plane with respect to which the brain exhibits maximum symmetry. Practically, this approximate symmetry plane is to be close to the fissure, but is computed using the whole 3D image and no anatomical landmarks.

Methods. In some algorithms [1, 18, 20], the searched plane is parameterized, the symmetric of the original image is computed according to the current parameters, and a similarity measure is computed between the 2 resulting images. The rigid transformation aligning the plane giving the maximum similarity with the center of the image lattice is derived straightforwardly. In other algorithms [9, 12], a rigid transformation correctly aligning the unknown plane is directly searched. Two rotations (axial and coronal) and one translation (along the left-right axis) are theoretically enough to perform this task, and constitute the unknown parameters. The original image is rotated and centered according to the current parameters, then flipped with respect to the center of the image lattice (which is then supposed to be the searched mid-sagittal plane), and a similarity measure is computed between the rotated, centered image and its flipped version. In both cases, a search is completed across the set of parameters to achieve the maximum of the criterion.

Most often, the chosen similarity criterion is the cross-correlation. Generally, this criterion is computed between the intensities of the two symmetric 3D images [1]. A slightly different approach is presented in [9], where a 2D mid-sagittal axis is estimated for each coronal or axial slice, and a 3D plane is deduced from the set of these lines, following geometrical considerations as in [3]. For a given slice, the selected axis is the line that maximizes the cross-correlation between the two reflected images with respect to this line. The main drawback of this method is that when the head is strongly tilted, the

homologous anatomical structures or functional areas in both hemispheres are not displayed in the same coronal or axial slices: the mid-sagittal lines are likely to be meaningless. Thus, if the axes are computed on the coronal (resp. axial) slices, this approach requires the correction of the yaw (resp. roll) angle a preprocessing. The method described in [8] is basically the same, but limited to 2D axial slices (no 3D plane is computed), and applied to other modalities (see Table 1 for details).

Instead of intensities, the criterion can be computed from features derived from the original image. In [19, 20], the gradient orientation histogram is computed, and its values are reported on a tessellated unit sphere, giving the Extended Gaussian Image (EGI). Theoretically, if the brain is symmetrical, so is its EGI. The direction of the symmetry plane is the one that maximizes the correlation of the two flipped versions of the EGI with respect to this plane, within the discrete set of orientations defined by the tessellation. As a preprocessing, the image is rotated and centered according to the principal axes and the center of mass of the head. The resolution is limited to the tessellation of the unit sphere, and to well contrasted images (CT and MR), due to the computation of the gradient.

Contrary to the first class of methods, the whole 3D volume is taken into account, which means that the overall gross symmetry of the brain is used. Consequently, these methods are less sensitive to the variability of the inter-hemispheric fissure and its curved shape. The trade-off is the need for the criterion to be robust with respect to departures from the gross underlying cerebral symmetry, i.e., the normal and pathological asymmetries of the brain. This robustness is difficult to achieve with global criteria such as the cross-correlation, that is affected in the same way by areas in strong (i.e., symmetrical) and weak (i.e., asymmetrical) correlation. These latter can severely bias the estimation of the plane [1]. Actually, the implicit hypothesis underlying these methods is that the two sides of the brain are not too dissimilar.

To overcome this issue, another similarity criterion is proposed in [12]: the stochastic sign change, which was previously shown to be efficient in case of rigid registration, even for quite dissimilar images [25, 5]. In the same way, a new symmetry measure introduced in [18] allows to take into account mainly strongly symmetrical parts of the brain. First, an optimal plane is computed within the set of planes with the same normal: for each line with this orien-

tation in the image, a center of symmetry is identified in its intensity profile, by maximization of a criterion which is equal to 1 (resp. -1) in case of perfect symmetry (resp. antisymmetry). The plane best fitting the set of centers and a symmetry criterion attached are subsequently derived, giving more strength to centers with respect to which the lines exhibit strong symmetry. The mid-sagittal plane is the plane with maximal symmetry criterion among all the possible orientations.

Advantages & drawbacks. The main drawback of this global approach, as previously noted, is its sensitivity to asymmetries deviating from the underlying gross symmetry of the brain. We mainly aim at tackling this issue in this paper. Another drawback of these methods is the computational cost of the algorithms, due to the optimization scheme within the set of possible planes. However, this cost can be often reduced: the discretization of the parameters space (that limits the accuracy of the results) or a prior knowledge about the position of the optimal plane allow to investigate only a limited number of planes. Thus, the reorientation of the principal axes of the brain and the centering of its center of mass is often a useful preprocessing step. A multi-resolution scheme can also accelerate the process [1]. The main advantage of these approaches is their ability to tackle other modalities than MR, in particular functional images: results on CT, PET, and SPECT images are presented in the cited papers.

Methods	Based on...	Applications
Brummer, 91 [3]	inter-hemispheric fissure	MR
Guillemaud *et al.*, 95 [7]	inter-hemispheric fissure	MR
Ardenaki *et al.*, 97 [1]	symmetry criterion	MR, PET
Smith *et al.*, 99 [18]	symmetry criterion	MR, CT, PET, SPECT
Sun *et al.*, 97 [20]	symmetry criterion	MR, CT
Liu *et al.*, 98 [9]	symmetry criterion	MR, CT
Junck *et al.*, 90 [8]	symmetry criterion	PET, SPECT
Minoshima *et al.*, 92 [12]	symmetry criterion	PET

Table 1: Summary of the main features of existing methods.

1.3 Overview of the paper

In this paper, we present a new symmetry-based method allowing to compute, reorient and recenter the mid-sagittal plane in anatomical and functional images of the head. This method, generalizing an approach previously described in recent papers [23, 14, 24], is composed of two steps. At first, the computation of local rather than global similarity measures between the two sides of the brain (or the skull in CT images) allows to match homologous anatomical structures or functional areas, by way of a block matching procedure. The output is a set of point-to-point correspondences: the centers of homologous blocks. Subsequently, we define the mid-sagittal plane as the one best superposing the points in one hemisphere and their counterparts in the other hemisphere by reflective symmetry. The estimation of the parameters characterizing the plane is performed by a least trimmed squares optimization scheme. Then, the estimated plane is aligned with the center of the image lattice. This method is fully automated, objective and reproducible.

This approach allows to deal with two severe drawbacks of classical symmetry-based methods. First, the computation of local measures of symmetry and the use of a robust estimation technique [17] allow to discriminate between symmetrical and asymmetrical parts of the brain or the skull. Practically, the mid-sagittal plane is mainly computed from the underlying gross symmetry of the head, because its estimation is robust with respect to normal or abnormal asymmetries which are treated as outliers. Second, the regression step yields an analytical solution, computationally less expensive than optimization schemes based on an exhaustive search.

We extensively describe this new approach in section 2. In section 3, we show that we are able to cope with strongly asymmetrical and tilted head or brain, even in presence of noise and bias, with very good accuracy and low computation time. In section 4, we present results on anatomical (MR, CT) and functional (PET, SPECT) images.

2 Description of the method

2.1 Presentation of the main principles

As an introduction, we recall the principles of the method presented in [23, 14, 24]. Given I, an MR image of the head, the mid-sagittal plane P is defined as the one best superposing the pairs $\{a_i, S_P(b_i)\}$, where a_i is a brain voxel, b_i its anatomical counterpart in the other hemisphere, and S_P the symmetry with respect to the searched plane P. In concrete terms, P is obtained by minimization of the least squares (LS) criterion $\sum_i ||a_i - S_P(b_i)||^2$, where $||.||$ is the Euclidian norm. An analytical solution of this problem is described in the appendix. The pairs $\{a_i, b_i\}$ are obtained as follows (see also Figure 3):

- The mid-sagittal plane K of the image lattice (K is considered to be fixed to the grid) differs from the searched mid-sagittal plane P of the brain in the tilt of the head during the scanning process, but is usually a good first estimate. The original image I is flipped with respect to K, giving the image $S_K(I)$.
- The "demons" algorithm [22] finds the anatomical counterpart b'_i in $S_K(I)$ of each point a_i in I, by way of non-rigid registration between the 2 images.
- The symmetric of b'_i with respect to K is the anatomical counterpart (noted b_i) of a_i in the other hemisphere: $b_i = S_K(b'_i)$. For example, in I, the point at the top of the right ventricle is matched with the point at the top of the left ventricle.

After P is computed, the transformation $R = S_K \circ S_P$ is a rotation if P and K are not parallel and a translation if P and K are parallel. It is shown that the transformation $R^{1/2}$, when applied to the image I, automatically aligns the plane P with K. Several difficulties and limitations arise when using this method:

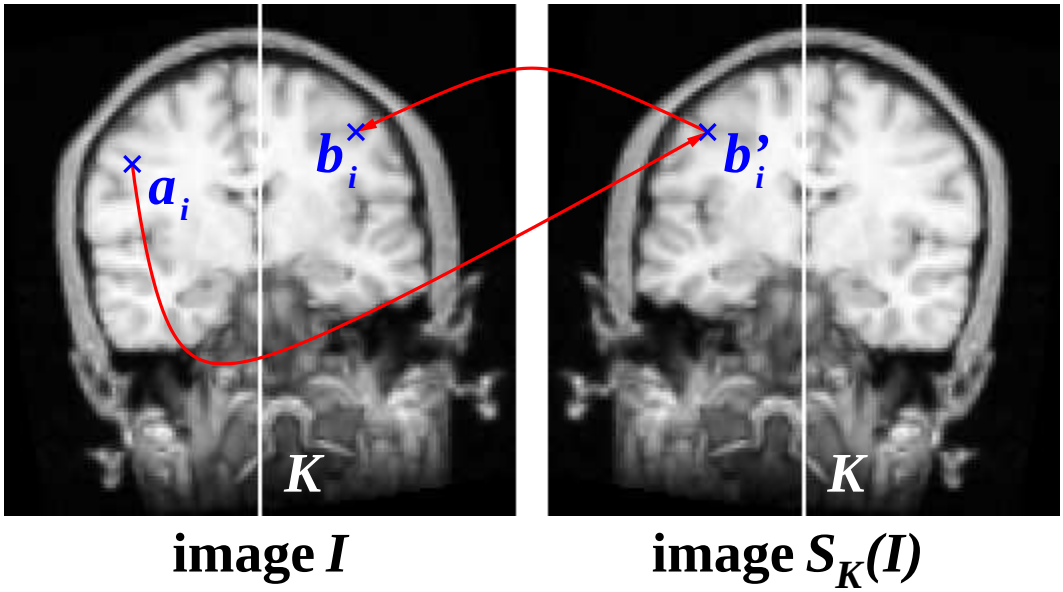

Figure 3: **The non-rigid registration strategy**. The point b'_i in $S_K(I)$ is matched with the point a_i in I; $b_i = S_K(b'_i)$ is the counterpart of a_i in the other hemisphere.

- As many of the classical symmetry-based methods, normal and pathological asymmetries can severely disrupt the computation of the plane. Even though it is based on local instead of global measures of symmetry, the minimization is performed on a global criterion, and will be strongly affected by the departures from the underlying symmetry. Actually, the least squares minimization is known to be not robust with respect to outliers [17].

- In addition, the non-rigid registration algorithm can provide aberrant matchings. When a structure is absent in one hemisphere (a lesion, one track of white matter, etc.), or when two structures are too different from each other, the matching is likely to fail, but these failures are difficult if not impossible to detect. Moreover, the matching process is performed on the whole image, in particular the background, event though the hypothesis of underlying symmetry is valuable only for head voxels. These meaningless correspondences will be systematically taken into account in the global least squares criterion.

- At last, the "demons" algorithm mainly relies on the gradient of the image, and proved to be efficient for high resolution and low-textured images like MR or CT. Consequently, this approach is difficult to extend to SPECT or PET images.

2.2 Modification based on a block matching strategy and a robust estimation technique

The modification we propose here allows to compute the mid-sagittal plane only from correspondences between very similar areas in both sides of the brain or the skull, i.e., very symmetrical areas, and to tackle both functional and anatomical images. The methodology is twofold, and basically the same as the one presented in the section 2.1. First, we find point-to-point correspondences between the two sides, and second, we find the plane best superposing the pairs of matched points. However, the matching and the optimization procedures are very different from [23, 14, 24].

2.2.1 Computation of inter-hemispheric correspondences by a block matching strategy

The pairs of correspondences $\{a_i, b'_i\}$ are obtained by way of a block matching strategy between the image I and its symmetric $S_K(I)$. This procedure is extensively described in [13] in case of rigid registration of anatomical sections. The common lattice of the 2 images (of size $X \times Y \times Z$) defines a set of rectangular parallelepipedic blocks of voxels $\{\mathcal{B}\}$ in I and $\{\mathcal{B}'\}$ in $S_K(I)$, given their size $N_x \times N_y \times N_z$: both images contain $(X - N_x + 1) \times (Y - N_y + 1) \times (Z - N_z + 1)$ such blocks. We aim at matching each block in $\{\mathcal{B}\}$ with the block in $\{\mathcal{B}'\}$ maximizing a given similarity measure, which yields a "displacement field" between I and $S_K(I)$. Practically, it is not computationally feasible to make an exhaustive search of matchings within $\{\mathcal{B}'\}$ for each block of $\{\mathcal{B}\}$. In addition, we have an *a priori* knowledge about the position of the correspondent $\mathcal{B}'$ of $\mathcal{B}$: if the head is not too tilted, $\mathcal{B}'$ is to be located in a neighborhood of $\mathcal{B}$. Thus we constrain the search procedure to subsets defined as follows:

- We limit the search for correspondences to one block $\mathcal{B}$ every Δ_x (resp. Δ_y, Δ_z) voxels in the x (resp. y, z) direction, defining a subset of $\{\mathcal{B}\}$; $\Delta = (\Delta_x, \Delta_y, \Delta_z)$ determines the density of the computed "displacement field" between I and $S_K(I)$.

- For each block $\mathcal{B}$ in this subset, we define a sub-image in $S_K(I)$, centered on $\mathcal{B}$, which delimits a neighborhood of research. This sub-image is composed of the voxels in $S_K(I)$ located within a distance of Ω_x (resp. Ω_y, Ω_z) voxels in the x (resp. y, z) direction from $\mathcal{B}$. This yields a rectangular parallelepipedic sub-image of size $(N_x + 2\Omega_x) \times (N_y + 2\Omega_y) \times (N_z + 2\Omega_z)$ in $S_K(I)$, which contains $(2\Omega_x + 1) \times (2\Omega_y + 1) \times (2\Omega_z + 1)$ blocks $\mathcal{B}'$ (provided this sub-image is entirely located in $S_K(I)$).

- In this sub-image, we examine one block $\mathcal{B}'$ every Σ_x (resp. Σ_y, Σ_z) voxels in the x (resp. y, z) direction; $\Sigma = (\Sigma_x, \Sigma_y, \Sigma_z)$ determines the resolution of the displacement field.

Note that the subset of $\{\mathcal{B}\}$ in I and the subset of $\{\mathcal{B}'\}$ in the sub-image of $S_K(I)$ contain respectively:

- $\max\{n_x | (n_x - 1)\Delta_x + N_x \leq X\} \times$
  $\max\{n_y | (n_y - 1)\Delta_y + N_y \leq Y\} \times$
  $\max\{n_z | (n_z - 1)\Delta_z + N_z \leq Z\}$ and
- $\max\{n_x | (n_x - 1)\Sigma_x \leq 2\Omega_x\} \times$
  $\max\{n_y | (n_y - 1)\Sigma_y \leq 2\Omega_y\} \times$
  $\max\{n_z | (n_z - 1)\Sigma_z \leq 2\Omega_z\}$ blocks

We note $\mathcal{B}_{ijk}$ (resp. $\mathcal{B}'_{lnm}$) the block in I (resp. $S_K(I)$) containing the voxel (i, j, k) (resp. (l, n, m)) at its top left back corner. We summarize the features of the algorithm as follows:

- For $(i = 0; i \leq X - N_x; i = i + \Delta_x)$
- For $(j = 0; j \leq Y - N_y; j = j + \Delta_y)$
- For $(k = 0; k \leq Z - N_z; k = k + \Delta_z)$
- We consider the block $\mathcal{B}_{ijk}$ in I
  - For $(l = i - \Omega_x; l \leq i + \Omega_x; l = l + \Sigma_x)$
  - For $(m = j - \Omega_y; m \leq j + \Omega_y; m = m + \Sigma_y)$
  - For $(n = k - \Omega_z; n \leq k + \Omega_z; n = n + \Sigma_z)$
  - If the block $\mathcal{B}'_{lnm}$ in $S_K(I)$ is entirely located in the image lattice, we compute a similarity measure with $\mathcal{B}_{ijk}$
- We retain the block $\mathcal{B}'_{lnm}$ with maximal similarity measure, which defines the displacement vector between the center $(i+N_x/2, j+N_y/2, k+N_z/2)$ of $\mathcal{B}_{ijk}$ and the center $(l + N_x/2, n + N_y/2, m + N_z/2)$ of $\mathcal{B}'_{lnm}$.

Thus, a given choice of parameters $N = (N_x, N_y, N_z)$, $\Omega = (\Omega_x, \Omega_y, \Omega_z)$, $\Delta = (\Delta_x, \Delta_y, \Delta_z)$, $\Sigma = (\Sigma_x, \Sigma_y, \Sigma_z)$, whose interpretation will be given in section 2.2.3, yields pairs of correspondences (a_i, b'_i) between I and $S_K(I)$, a_i and b'_i being the centers of matched blocks. The output of this scheme is a displacement field, which conveys local information about brain symmetry and asymmetry. The points $\{b'_i\}$ are then flipped back with respect to K, giving the points $\{b_i = S_K(b'_i)\}$. The point b_i is the counterpart of a_i in the opposite side of the head (see Figure 4).

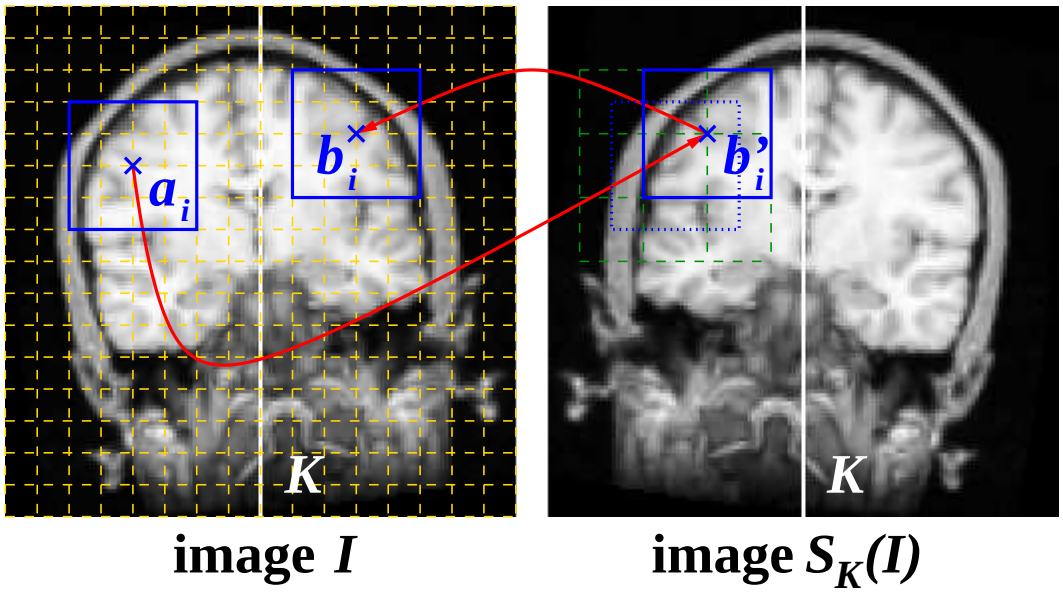

Figure 4: **The block matching strategy**. The point b'_i in $S_K(I)$ is homologous to the point a_i in I; $b_i = S_K(b'_i)$ is the counterpart of a_i in the other hemisphere. We display coronal slices of the brain. I contains 128^3 voxels and the chosen parameters are: $N = (32, 32, 32)$, $\Delta = (8, 8, 8)$, $\Omega = (8, 8, 8)$, $\Sigma = (16, 16, 16)$. In I, the subset of $\{\mathcal{B}\}$ is defined by the gold grid (parameters Δ). Around the blue block of center a_i, superposed on $S_K(I)$ (in blue with dotted line), a neighborhood of research is delimited (parameters Ω). In this sub-image of $S_K(I)$, the search is completed on the subset of $\{\mathcal{B}'\}$ defined by the green grid (parameters Σ). In this case, for each of the $13^3 = 2197$ such defined blocks in I, the search is done on $2^3 = 8$ blocks in $S_K(I)$.

Different criteria can be chosen as a similarity measure, such as the classical Correlation Coefficient (CC), also called the normalized cross-correlation [2], the Correlation Ratio (CR) [16] or the Mutual Information (MI) [26, 10]. Each of these measures assumes an underlying relationship between the voxel intensities of the 2 images, respectively affine (CC), functional (CR), or statistical (MI) [15]. Practically, the CR and the MI are well suited to multi-modal registration, whereas the CC is suited to monomodal registration. In our case, the CC turns out to be sufficient: an affine, or locally affine relationship can be assumed between I and $S_K(I)$, which have the same "modality". If we consider a block $\mathcal{B}$ in I, with voxels of intensities $x_1, ..., x_n$, and a block $\mathcal{B}'$ in $S_K(I)$, with voxels of intensities $y_1, ..., y_n$, the CC between $\mathcal{B}$ and $\mathcal{B}'$ is equal to:

$$CC = \frac{\frac{1}{n}\sum_{i=1}^{n}(x_i-\bar{x})(y_i-\bar{y})}{\frac{1}{n}\sqrt{\sum_{i=1}^{n}(x_i-\bar{x})^2\sum_{i=1}^{n}(y_i-\bar{y})^2}} = \frac{\overline{xy}-\bar{x}\bar{y}}{\sigma(x)\sigma(y)}, \text{ in terms of random variables}$$

It can be easily shown that $-1 \leq CC \leq 1$. The CC measures the strength of the affine relationship between $\mathcal{B}$ and $\mathcal{B}'$. In particular, if |CC|=1, there exist coefficients a and b such that $y_i = ax_i + b$ for all the voxels $i = 1, ..., n$ in these blocks. Thus, we aim at maximizing |CC|. Contrary to methods based on a global criterion, this new approach allows to eliminate very asymmetrical and meaningless areas from the computation of the plane by using local measures of symmetry. First, if no block $\mathcal{B}'$ in the subset defined in $S_K(I)$ exhibits a high |CC| with a given block $\mathcal{B}$ in the subset defined in I, its center is eliminated straightforwardly, by setting a convenient threshold. In practice, this happens when the structures existing in one given block in I are absent from any block in $S_K(I)$, which is the case for strongly asymmetrical areas. This elimination is not easily feasible in [23, 14, 24], where it is difficult to detect where the non-rigid algorithm fails. Second, background voxels are naturally ignored in this framework, because we eliminate blocks with low variance from the optimization process. Thus, the estimation step, performed with these preselected inter-hemispheric correspondences, is mainly based on symmetrical areas. The robust estimation technique we use (a least trimmed squares minimization) allows to eliminate the remaining asymmetrical areas from the computation of the plane.

2.2.2 Computation of the mid-sagittal plane by a least trimmed squares minimization

A least trimmed squares (LTS) strategy is used to find the plane P best superposing the points $\{a_i\}$ and their counterparts $\{b_i\}$. This minimization scheme has been proven to be far more robust to outliers than the classical least squares method [17]. Actually, in our problem, we have to deal with two kinds of outlying measures. First, depending on the choice of the parameters, aberrant matchings can happen if the head is strongly tilted. Second, even after the initial short-listing that eliminates blocks with low |CC| , blocks conveying strong asymmetries can remain. This happens when two structures are present in both hemispheres, but in different locations: the two matched blocks containing this structure exhibit a high |CC| . The use of a robust minimization technique enables the computed plane to be only based on the underlying gross symmetry of the brain, the asymmetries being treated as outliers. The LTS scheme we use is:

- The plane P minimizing $\sum_i ||a_i - S_P(b_i)||^2$ is analytically found, as described in the appendix; $||.||$ is the Euclidian norm.
- The residuals $r_i = ||a_i - S_P(b_i)||$ are trimmed, and P is recomputed as previously, using only the voxels i with the 50% smaller residuals.
- When the angle between the normal vectors of two successively estimated planes is lower than a fixed threshold, we consider that they are "sufficiently close" to each other, and the iterative scheme stops.

This strategy is able to cope with up to 50% of outliers (i.e., a breakdown point of 0.5) [17]. To improve the accuracy of the estimation, we iterate the process (Figure 5). As previously noted, the transformation $R = (S_K \circ S_P)^{1/2}$ is such that $P = K$ in $R(I)$. We make a new block matching between $R(I)$ and $S_K(R(I))$, K being the firstly estimated plane P, and a new estimation P_2 of the mid-sagittal plane by the LTS procedure. The transformation $R_2 = (S_K \circ S_{P_2})^{1/2} = (S_P \circ S_{P_2})^{1/2}$ is such that $P_2 = K$ in $R_2 \circ R(I))$. After several iterations, the mid-sagittal plane P_n is computed from the image $(R_{n-1} \circ ... \circ R_2 \circ R)(I)$. The final estimate is the plane K in $(R_n \circ ... \circ R)(I)$. The composition

of the successively estimated rigid transformations avoids multiple resampling and loss of data information. Usually, we choose a fixed number of iterations.

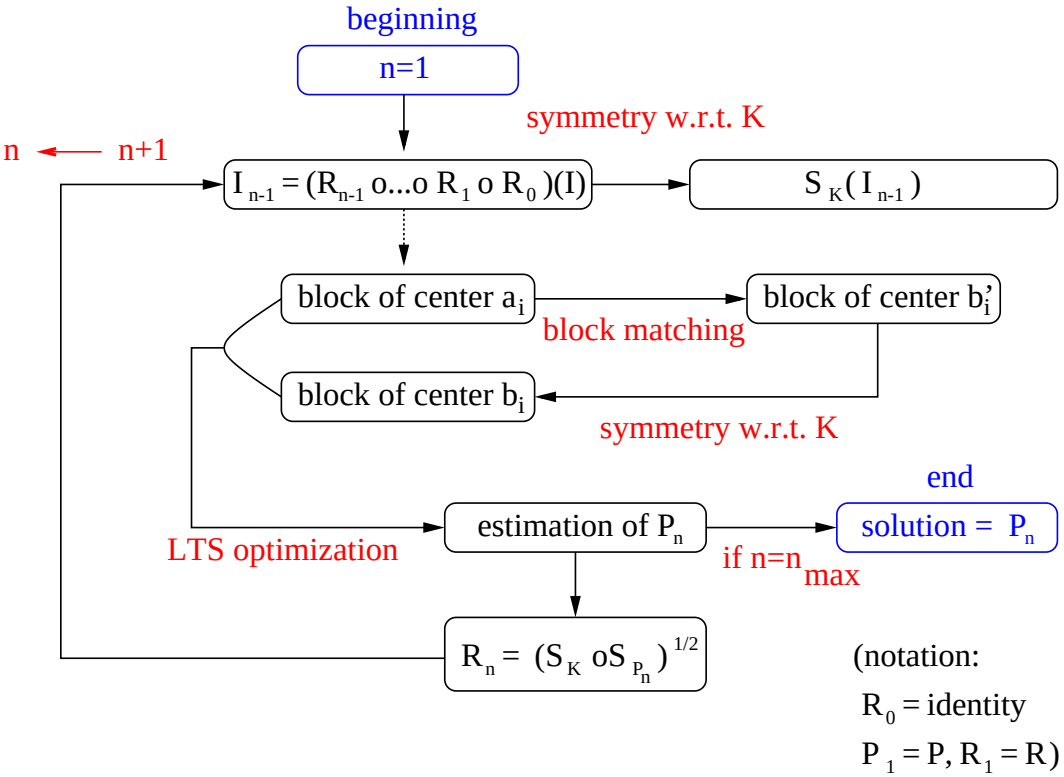

Figure 5: **General scheme**. We describe the iterative process for one given choice of parameters (i.e., at one given scale). Usually, we fix the number of iterations: typically, $n_{max} = 5$ yields good results (see section 3).

2.2.3 Multiscale scheme

Given a set of parameters N, Ω, Δ, Σ, the complexity of the block matching process is proportional to $\frac{(N_x N_y N_z)(\Omega_x \Omega_y \Omega_z)}{(\Delta_x \Delta_y \Delta_z)(\Sigma_x \Sigma_y \Sigma_z)}$ [13]. Intuitively, when I is strongly tilted, I and $S_K(I)$ are far from each other, and the neighborhood of research

must be large (parameters Σ), to deal with strong differences in translation and rotation. In this case, we also expect large windows (parameters N) to give more meaningful CC than small ones. This implies a large computational cost. On the contrary, when I is already well aligned, we can restrict the neighborhood of research, and trust more the CC computed on small windows.

We implemented a multiscale scheme to achieve a good trade-off between accuracy and complexity. Initially, when the head is suspected to be strongly tilted, we make a first estimation of the mid-sagittal plane with large values of N, Ω, Δ, Σ, based on a displacement field with low density and low resolution. This estimate P_n^1 is the center of $(R_n^1 \circ ... \circ R^1)(I)$ (n is the number of iterations at a given scale, see section 2.2.2). Then, we decrease the parameters so that the complexity remains constant, the new estimate P_n^2 is the center of $(R_n^2 \circ ... \circ R^2 \circ R_n^1 \circ ... \circ R^1)(I)$, and so on. At the last scale, the estimation is based on a displacement field of high density and high resolution, and is likely to be accurate. Practically, we make the following usual choices for isotropic as well as anisotropic images:

- The initial values of the parameters are:
  - $N = ([X/4], [Y/4], [Z/4])$ or $N = ([X/8], [Y/8], [Z/8])$ (discussed in the next section)
  - $\Omega = N$, $\Delta = \Sigma = N/4$
- At each iteration, they are automatically updated as follows:
  $N \leftarrow N/2$, $\Omega \leftarrow \Omega/2$, $\Delta \leftarrow \Delta/2$, $\Sigma \leftarrow \Sigma/2$.
- The updating in the direction x (resp. y, z) stops when N_x (resp. N_y, N_z) is smaller than 4 at the next scale. At this level, the small block size makes the computed CC become meaningless. The whole process stops when there is no updating in any direction. For an image of size 128^3 and for each of the 2 choices we usually make for initial parameters, we get 4 and 3 scales respectively, and $\Delta = \Sigma = (1, 1, 1)$ at the last scale: this means that we obtain a displacement field of high density and resolution.

3 Validation: robustness and accuracy analysis

3.1 Materials

In this section, we present a series of validation experiments on simulated data, to show the robustness and the accuracy of the algorithm. Moreover, we aim at finding a set of optimal parameters for the computation of the plane and showing that the algorithm is robust with respect to a relatively high level of bias. The total simulated dataset is composed of 1152 synthetic MR images, generated as follows.

First, a perfectly symmetrical image I_1 is created. We consider an original MR image I of size 256^3, with voxel size 0.78mm^3, provided by Dr. Neil Roberts, Magnetic Resonance and Image Analysis Research Centre (University of Liverpool, UK). Running our algorithm directly on high resolution images leads to a prohibitive computation time; we resample I to get a new image of size 128^3. In this latter, a mid-sagittal plane is determined by visual inspection, and matched with the center of the image lattice. One half of the brain is removed, and the other half is flipped with respect to the center. The center of this image I_1 is a perfect symmetry plane, and constitutes the ground truth for our validation experiments.

Second, artificial lesions (or tumors) with different grey levels and local expansions and shrinkings are added inside the brain to create strong focal asymmetries. Third, an additive, stationary, Gaussian white noise (standard deviation of 3) is added, on top of the "natural" noise of the original MR image. Fourth, a roll, a yaw angle and a translation along the left-right axis is applied. We choose the angles in the set {0, 3, 6,..., 21} (in degrees), and the translations in the set {0, 4, 8,..., 20} (in voxels): the 384 possible combinations constitute the **dataset A**; note that the applied noise is different in each image. By resampling I_1 to the size 64^3, we get the image I_2. Adding the same lesions, deformations and random noise in I_2, applying the same rotations, and translations of 0, 2,..., 10 voxels (note that the transformation with parameters (yaw,roll,translation)$=(\alpha, \beta, 2t)$ in dataset A and (α, β, t) in dataset B are the same), we get a second dataset of 384 images (**dataset B**). At last, a strong multiplicative bias field (linear in x, y and z) is added to

I_2 before applying the transform, which creates a third dataset of 384 images (**dataset C**). In brief, we get the 3 following datasets:

- dataset A: I_1 + lesions + deformations + noise + 2 rotations + 1 translation
- dataset B: I_2 + lesions + deformations + noise + 2 rotations + 1 translation
- dataset C: I_2 + lesions + deformations + noise + bias + 2 rotations + 1 translation

3.2 Methods

For these 3 datasets, we run the program as follows:

- Experiment 1: dataset A with $(N, \Omega, \Delta, \Sigma) = (32, 32, 8, 8)$, 5 iterations at each scale
- Experiment 2: dataset A with $(N, \Omega, \Delta, \Sigma) = (16, 16, 4, 4)$, 5 iterations at each scale
- Experiment 3: dataset B with $(N, \Omega, \Delta, \Sigma) = (16, 16, 4, 4)$, 5 iterations at each scale
- Experiment 4: dataset C with $(N, \Omega, \Delta, \Sigma) = (16, 16, 4, 4)$, 5 iterations at each scale

For each of these experiments, the computed roll, yaw angles and translation along the left-right axis aligning the estimated mid-sagittal plane are compared with the applied ones, giving a measure of **accuracy** of the algorithm. For this purpose, the computed rigid transform is composed with the applied one. The norm of the yaw and roll angles of the rotation component of this composition and the norm of its translation along the left-right axis are computed; the closer to zero these 3 parameters are, the more accurate the result is. Another measure of accuracy ϵ is described in Figure 6. We consider that an experiment is successful when ϵ is lower than a given threshold, typically, 1 voxel. We search the maximal value of δ (which measures the initial

tilt of the head, see Figure 6) for which the algorithm succeeds. This value δ_{max} gives an idea of the **robustness** of the algorithm.

Comparing the experiments 1 and 2 (resp. 1 and 3) shows the influence of the initial size of the blocks (resp. subsampling) on the accuracy, the robustness and the computation time of the algorithm. This aims at indicating which set of parameters is best adapted to real medical images. Comparing the experiments 3 and 4 shows the sensitivity of the algorithm to a relatively high bias. The experiments were led on a standard PC (OS Linux), 450 MHz, 256 MBytes of RAM.

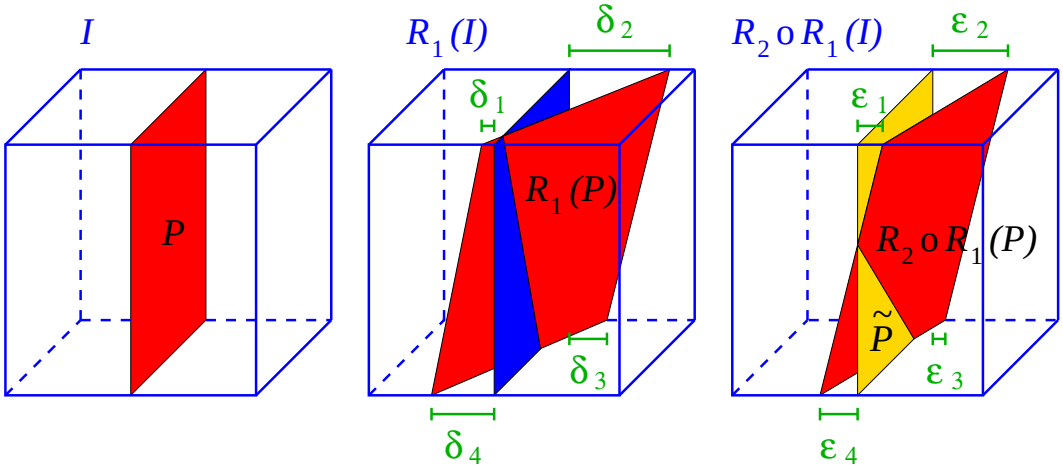

Figure 6: **A measure of accuracy**. A synthetic image I is generated, in which the red plane P is the sought mid-sagittal plane of the brain, as described in the text (left sketch). We apply yaw, roll angles, and a translation along the left-right axis, which yields a rigid transformation R_1. In $R_1(I)$, the real mid-sagittal plane $R_1(P)$ is no longer aligned with the center (in blue) of the grid (central sketch). The maximum δ of the four distances $\delta_1, \delta_2, \delta_3, \delta_4$, measure the tilt of the head before we run the algorithm on the image $R_1(I)$. We estimate a mid-sagittal plane $\tilde{P}$ and a rigid transformation R_2 so that $\tilde{P}$ is displayed in the center of $R_2 \circ R_1(I)$ (right sketch). The estimated plane $\tilde{P}$ (in gold) is generally different from the real one $R_2 \circ R_1(P)$ (in red). A measure of error is the maximum ϵ of the four distances $\epsilon_1, \epsilon_2, \epsilon_3, \epsilon_4$, which gives an idea of the maximal error in the whole volume of the image.

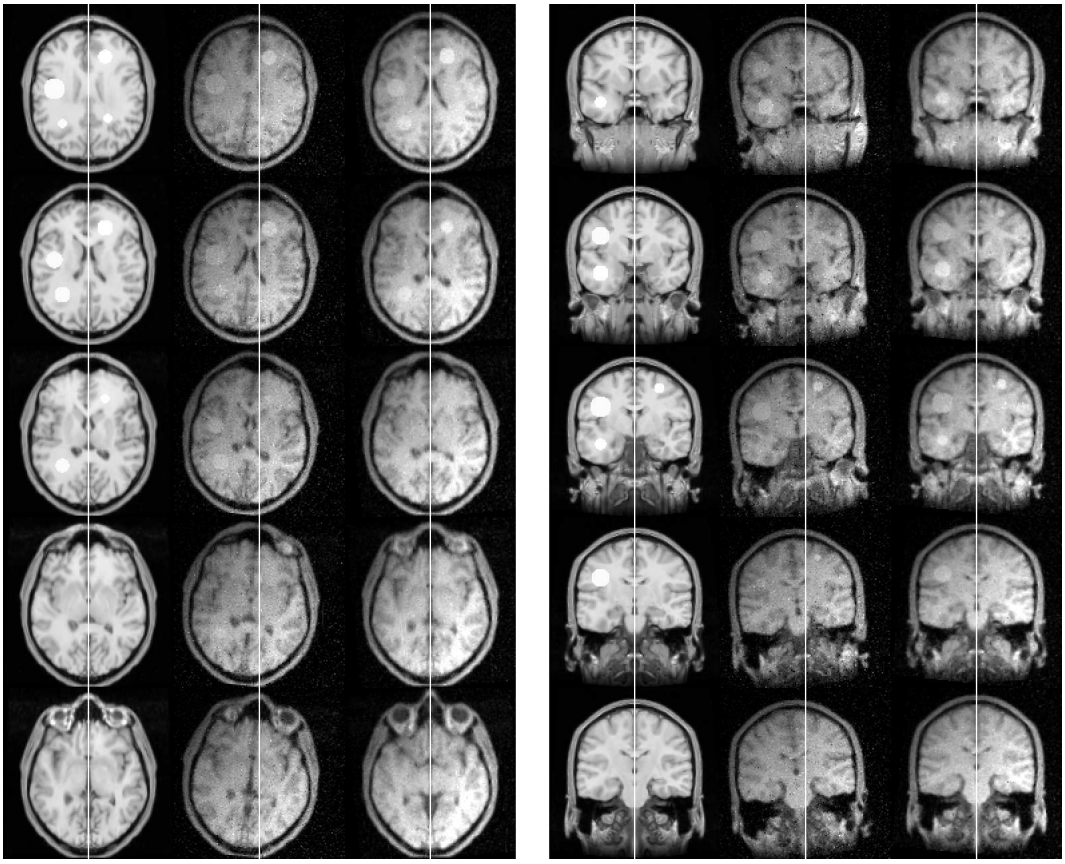

Figure 7: **Realignment of a synthetic MR image**. Artificial lesions, local deformations, noise and bias are added to a perfectly symmetrical MR image of size 128^3. Roll and yaw angles of 6 degrees, and translation along the left-right axis of 6 voxels are applied to this image. The initial parameters of the block matching algorithm are $(N, \Omega, \Delta, \Sigma) = (16, 16, 4, 4)$. The errors of the computed transform, compared to the applied one are: 4.10^{-2} degrees (roll angle), 3.10^{-2} degrees (yaw angle), 10^{-1} voxels (translation), and 2.10^{-1} voxels (error ϵ, see Figure 6). We display 2 panels with axial (left) and coronal (right) views. In each panel, from left to right, we have the original image with added lesions and deformations, the tilted image with added noise and bias, and the realigned image.

3.3 Results and interpretation

Experiment 1 vs 2. The algorithm proved to be highly robust for the experiment 1. It never failed when δ was lower than 51 voxels, which corresponds (for example) to parameters (yaw,roll,translation)=$(15, 15, 16)$, $(18, 18, 8)$ or $(21, 21, 0)$. In real images, the tilt of the head is usually smaller. We noticed that the convergence of the algorithm is the same for parameters (α, β, t) and (β, α, t): the yaw and roll angles play symmetric roles. Note that this convergence is not deterministic in our experiments, because the random noise is added separately on each image of the datasets. Thus, the algorithm did not fail systematically for more extreme parameters; for example, it succeeded for the parameters $(21, 21, 20)$. For the experiment 2, the rate of success is significantly reduced: it systematically succeeded when δ was lower than 42, which approximately corresponds to parameters $(12, 12, 16)$, $(15, 15, 18)$ or $(18, 18, 0)$. The small initial block size and the restricted neighborhood of research explain that the algorithm is unable to deal with too tilted heads. Compared to experiment 1, there is one less scale to explore, and the average computation time is reduced, but still prohibitive (about 34 min). The obtained accuracy is about the same compared to experiment 1. As a conclusion, the set of initial parameters $N = ([X/4], [Y/4], [Z/4])$ seems to be best adapted at a given resolution of the image.

Experiment 1 vs 3. For these two datasets, studied with optimal initial block size, the robustness is about the same, surprisingly. The subsampling does not reduce significantly the efficiency of the algorithm, which can fail when δ is superior to 25 voxels, which corresponds to parameters $(15, 15, 8)$, $(18, 18, 4)$ or $(21, 21, 0)$, comparable with the parameters of experiment 1. The accuracy is divided by two in experiment 3 compared to experiments 1 and 2, but remains very high (see Table 2). At last, the computation time is strongly reduced (by a factor of 10). This suggests that highly subsampled images (from 256^3 to 64^3) are enough for a satisfying reorientation and recentering.

Experiment 3 vs 4. The algorithm is very robust with respect to a relatively high bias. This is an important feature of this local approach. Locally, the intensity variations are smaller than on the whole image, and the CC is still a sensible measure. The accuracy and the computation time are similar between experiments 3 and 4.

Exp.	Robustness (δ_{max})	Accuracy (RMS errors)				CPU Time
		Roll Angle	Yaw Angle	Translation	ϵ	
1	51 voxels	4.10^{-2}	4.10^{-2}	5.10^{-2}	11.10^{-2}	$45'$
2	42 voxels	3.10^{-2}	4.10^{-2}	5.10^{-2}	10.10^{-2}	$34'$
3	25 voxels	11.10^{-2}	9.10^{-2}	6.10^{-2}	13.10^{-2}	3'
4	25 voxels	11.10^{-2}	8.10^{-2}	7.10^{-2}	11.10^{-2}	$3'$

Table 2: **Results**. The RMS errors (indicated for successful experiments only) are measured in degrees for the angles and voxels for the left-right translation and the value ϵ (see Figure 6). The errors are doubled between experiments on 128^3 and 64^3 images, including for the translation and ϵ (the errors in voxels are about the same, and the errors in mm are doubled for half resolution images).

Conclusion. In brief, we can draw several conclusions from these experiments: the accuracy is always very high when the algorithm succeeds. For a usual MR image of size 256^3, with voxel size 0.78mm^3 and with an initial tilt of δ lower than about 100 voxels, which corresponds to realistic conditions of $\delta = 50$ (resp. 25) voxels in the subsampled image of size 128^3 (resp. 64^3), our algorithm is likely to succeed. Applying it on the subsampled image of size 64^3, using $(16, 16, 4, 4)$ as initial parameters and doing 5 iterations at each scale, we reach a precision of about $\epsilon = 10.10^{-2} \times 4 \times 0.78 \simeq 0.3$ mm (see Table 2) for successful experiments (error computed as in Figure 6) within a CPU time of about 3 minutes. For strongly tilted images, an initial alignment along the principal axes of the head can be a useful preprocessing step.

4 Results on real medical images

In this section, we present results for real anatomical (MR, CT) and functional (SPECT, PET) images. For each illustration, we present axial (top) and coronal (bottom) views, for the initial 3D image (left) and the reoriented and recentered version (right). The MR image has been provided by Dr. Neil Roberts, Magnetic Resonance and Image Analysis Research Centre (University of Liverpool, UK), and is of size 256^3, with voxel size 0.78mm^3. The CT image comes from the Radiology Research Imaging Lab (Mallinckrodt Institute of Radiology, Saint Louis, Missouri, USA), and is of size $256 \times 256 \times 203$, with voxel size $0{,}6\text{mm}^3$. The SPECT image has been provided by Pr. Michael L. Goris, Department of Nuclear Medicine (Stanford University Hospital, USA), and is of size 64^3. At last, the PET image has been provided by the Hammersmith Hospital in London, UK, and the Unité 230 of INSERM, Toulouse, France. It is of size $128 \times 128 \times 15$, with voxel size $2.05\text{mm} \times 2.05\text{mm} \times 6.75\text{mm}$.

5 Conclusion

We have presented a new symmetry-based method allowing to compute, reorient and recenter the mid-sagittal plane in volumetric anatomical and functional images of the head. Our approach relies on the matching of homologous anatomical structures or functional areas in both sides of the brain (or the skull), and a robust estimation of the plane best superposing these pairs of counterparts. The algorithm is iterative, multiscale, fully automated, and provides a useful tool for further symmetry-based analysis of the brain. We showed on a large database of synthetic images that we could obtain a subvoxel accuracy in a CPU time of about 3 minutes, for strongly tilted heads, noisy and biased images. We have presented results on isotropic or anisotropic MR, CT, SPECT and PET images; the method will be tested on functional MR and ultrasound images in the future.

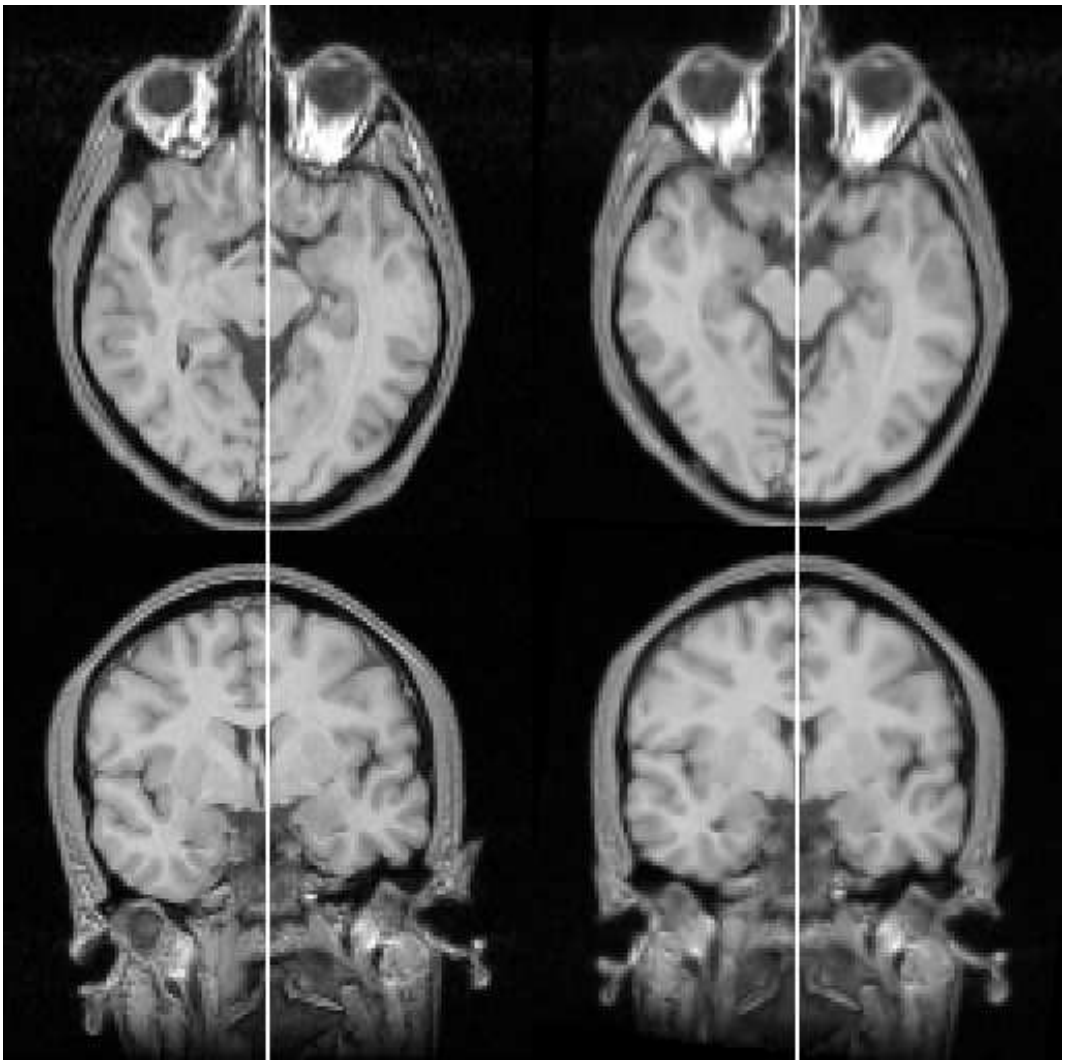

Figure 8: Isotropic MR image.

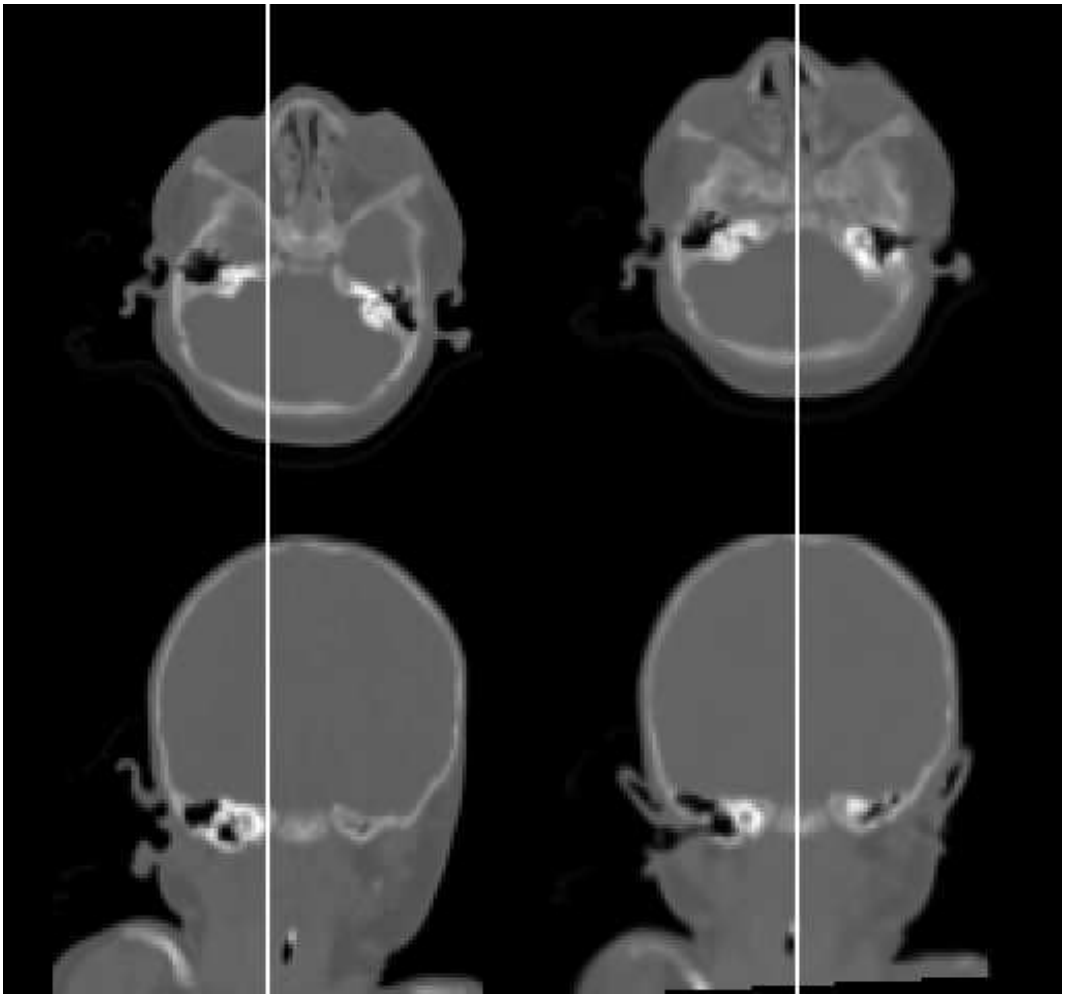

Figure 9: Isotropic CT image.

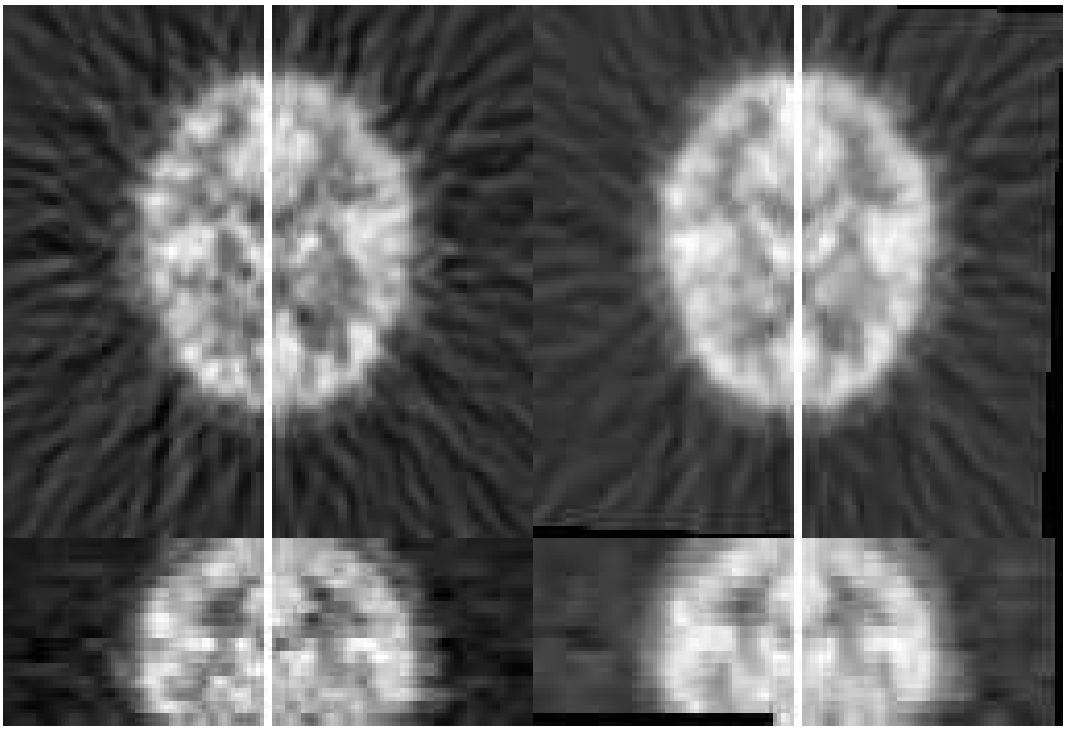

Figure 10: Anisotropic PET image.

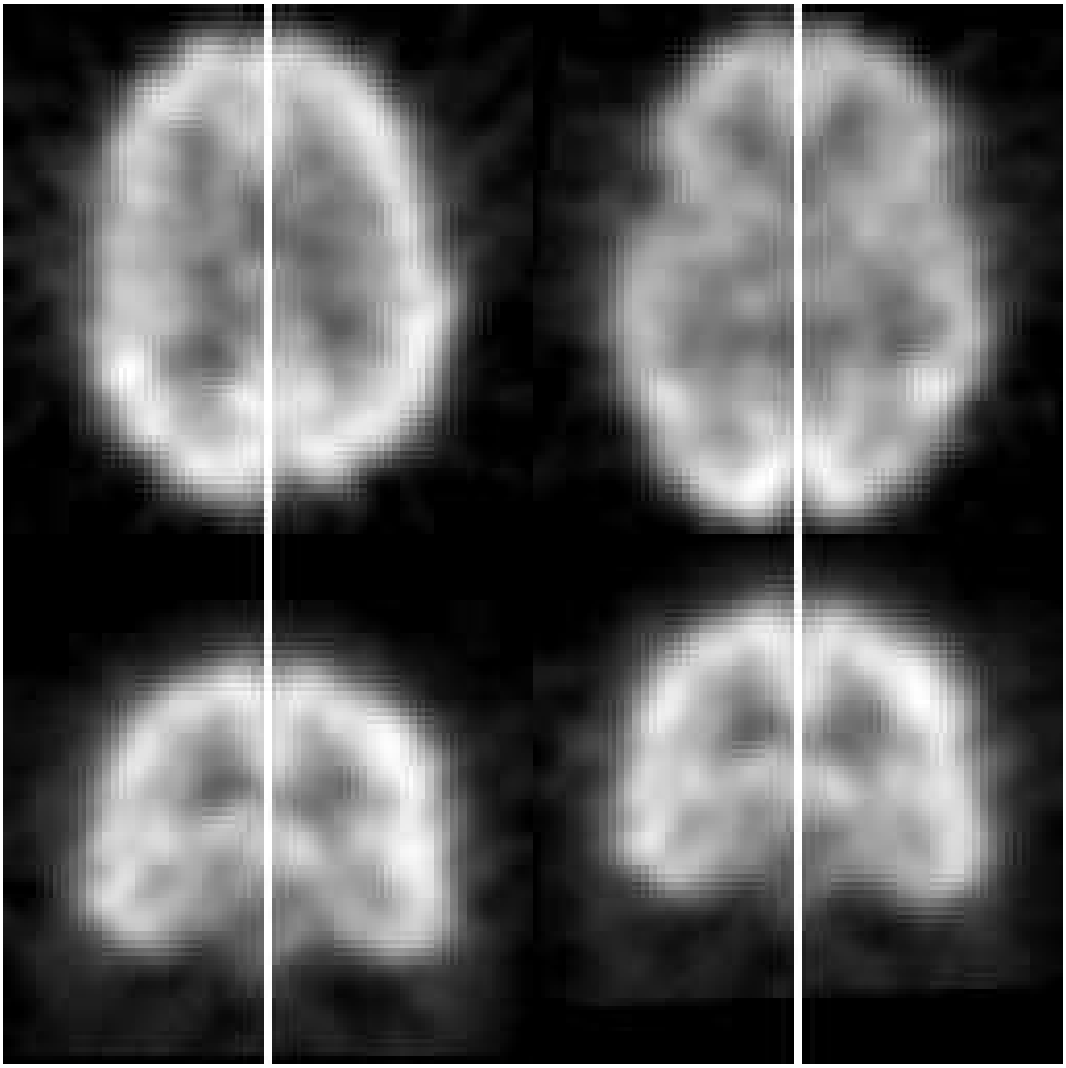

Figure 11: Isotropic SPECT image.

6 Appendix: mid-sagittal plane computation

We want to minimize:

$$C = \sum_i (S(b_i) - a_i)^2 \tag{1}$$

with $S(b_i) = b_i - 2((b_i - p)^\top n)n$ and where p is a point in the symmetry plane and n the unit normal vector to the plane. By differentiating C with respect to p, we get:

$$\frac{dC}{dp} = 4 \sum_i (2p - b_i - a_i)^\top n n^\top \tag{2}$$

which demonstrates that the barycenter G:

$$G = \frac{1}{n} \sum_i \frac{(b_i + a_i)}{2} \tag{3}$$

belongs to the symmetry plane. Substituting G in equation 1 and simplifying the equation, we get:

$$C = \sum_i (b_i - a_i)^2 + 4[(b_i - G)^\top n][(a_i - G)^\top n] \tag{4}$$

which is minimized when the following expression is minimized:

$$\sum_i n^\top [(a_i - G)(b_i - G)^\top] n \tag{5}$$

which means than n is the eigenvector associated to the smallest eigenvalue of I, where:

$$I = \sum_i (a_i - G)(b_i - G)^\top \tag{6}$$

References

[1] B.A. Ardenaki, J. Kershaw, M. Braun, and I. Kanno. Automatic Detection of the Mid-Sagittal Plane in 3-D Brain Images. *IEEE Transactions on Medical Imaging*, 16(6):947–952, December 1997.

[2] L.G. Brown. A survey of image registration techniques. *ACM Computing Surveys*, 24(4):325–375, December 1992.

[3] M.E. Brummer. Hough Transform Detection of the Longitudinal Fissure in Tomographic Head Images. *IEEE Transactions on Medical Imaging*, 10(1):74–81, March 1991.

[4] T.J. Crow. Schizophrenia as an anomaly of cerebral asymmetry. In K. Maurer, editor, *Imaging of the Brain in Psychiatry and Related Fields*, pages 1–17. Springer-Verlag, Berlin Heidelberg, 1993.

[5] P. Gerlot-Chiron and Y. Bizais. Registration of Multimodality Medical Images Using a Region Overlap Criterion. *CVGIP: Graphical Models and Image Processing*, 54(5):396–406, September 1992.

[6] N. Geschwind and W. Levitsky. Left-right asymmetry in temporal speech region. *Science*, 161:186–187, 1968.

[7] R. Guillemaud, A. Marais, P. amd Zisserman, B. McDonald, and T.J. Crow. A 3-Dimensional Midsagittal Plane For Brain Asymmetry Measurement. *Schizophrenia Research*, 18(2-3):183–184, 1995.

[8] L. Junck, J.G. Moen, G.D. Hutchins, M.B. Brown, and D.E. Kuhl. Correlation Methods for the Centering, Rotation, and Alignment of Functional Brain Images. *Journal of Nuclear Medicine*, 31:1220–1226, July 1990.

[9] Y. Liu, R.T. Collins, and W.E. Rothfus. Automatic Bilateral Symmetry (Midsagittal) Plane Extraction from Pathological 3D Neuroradiological Images. In *SPIE, International Symposium on Medical Imaging*, San-Diego, CA, February 1998.

[10] F. Maes, A. Collignon, Vandermeulen. D., G. Marchal, and P. Suetens. Multimodality Image Registration by Maximization of Mutual Information. *IEEE Transactions on Medical Imaging*, 16(2):187–198, April 1997.

[11] P. Marais, R. Guillemaud, M. Sakuma, A. Zisserman, and M. Brady. Visualising Cerebral Asymmetry. In Höhne, K.H. and Kikinis, R., editor, *Visualization in Biomedical Computing*, volume 1131 of *Lecture Notes in Computer Science*, pages 411–416, Hamburg (Germany), September 1996. Springer.

[12] S. Minoshima, K.L. Berger, K.S. Lee, and M.A. Mintun. An Automated Method for Rotational Correction and Centering of Three-Dimensional Functional Brain Images. *Journal of Nuclear Medicine*, 33:1579–1585, August 1992.

[13] S. Ourselin, A. Roche, G. Subsol, and X. Pennec. Automatic Alignment of Histological Sections. In F. Pernuš, S. Kovačič, H.S. Stiehl, and M.A. Viergever, editors, *International Workshop on Biomedical Image Registration, WBIR'99*, pages 1–13, Bled, Slovenia, August 1999. Electronic version: http://www.inria.fr/RRRT/RR-3595.html.

[14] S. Prima, J.-P. Thirion, G. Subsol, and N. Roberts. Automatic Analysis of Normal Brain Dissymmetry of Males and Females in MR Images. In W.M. Wells, A. Colchester, and S. Delp, editors, *First International Conference on Medical Image Computing and Computer-Assisted Intervention, MICCAI'98*, volume 1496 of *Lecture Notes in Computer Science*, pages 770–779, Boston, USA, October 1998. Springer.

[15] A. Roche, G. Malandain, N. Ayache, and S. Prima. Towards a Better Comprehension of Similarity Measures Used in Medical Image Registration. In C. Taylor and A. Colchester, editors, *Second International Conference on Medical Image Computing and Computer-Assisted Intervention, MICCAI'99*, volume 1679 of *Lecture Notes in Computer Science*, pages 555–566, Cambridge, USA, September 1999. Springer. Electronic version: http://www.inria.fr/RRRT/RR-3741.html.

[16] A. Roche, G. Malandain, X. Pennec, and N. Ayache. The Correlation Ratio as a New Similarity Measure for Multimodal Image Registration.

In W.M. Wells, A. Colchester, and S. Delp, editors, *First International Conference on Medical Image Computing and Computer-Assisted Intervention, MICCAI'98*, volume 1496 of *Lecture Notes in Computer Science*, pages 1115–1124, Boston, USA, October 1998. Springer. Electronic version: http://www.inria.fr/RRRT/RR-3378.html.

[17] P.J. Rousseuw and A.M. Leroy. *Robust Regression and Outlier Detection.* Wiley Series In Probability And Mathematical Statistics, 1987.

[18] S. Smith and M. Jenkinson. Accurate Robust Symmetry Estimation. In C. Taylor and A. Colchester, editors, *Second International Conference on Medical Image Computing and Computer-Assisted Intervention, MICCAI'99*, volume 1679 of *Lecture Notes in Computer Science*, pages 308–317, Cambridge, UK, September 1999. Springer.

[19] C. Sun. Symmetry detection using gradient information. *Pattern Recognition Letters*, 16:987–996, 1995.

[20] C. Sun and J. Sherrah. 3D Symmetry Detection Using The Extended Gaussian Image. *IEEE Transactions on Pattern Analysis and Machine Intelligence*, 19(2):164–168, 1997.

[21] J. Talairach and P. Tournoux. *Co-Planar Stereotaxic Atlas of the Human Brain.* Georg Thieme Verlag, 1988.

[22] J.-P. Thirion. Image matching as a diffusion process: an analogy with Maxwell's demons. *Medical Image Analysis (MedIA)*, 2(3):243–260, September 1998.

[23] J.-P. Thirion, S. Prima, G. Subsol, and N. Roberts. Statistical Analysis of Normal and Abnormal Dissymmetry in Volumetric Medical Images. In *IEEE Workshop on Biomedical Image Analysis, WBIA'98*, pages 74–83, Santa Barbara, USA, June 1998.

[24] J.-P. Thirion, S. Prima, G. Subsol, and N. Roberts. Statistical Analysis of Normal and Abnormal Dissymmetry in Volumetric Medical Images. *Medical Image Analysis (MedIA)*, 4(2), 2000. Electronic version: http://www.inria.fr/RRRT/RR-3178.html.

[25] A. Venot, J.F. Lebruchec, and J.C. Roucayrol. A New Class of Similarity Measures for Robust Image Registration. *Computer Vision, Graphics, and Image Processing*, 28(2):176–184, 1984.

[26] W.M. Wells III, P. Viola, H. Atsumi, S. Nakajima, and R. Kikinis. Multi-modal volume registration by maximisation of mutual information. In *Medical Image Analysis*, volume 1, pages 35–51. Oxford University Press, March 1996.

[27] T.H. Williams, N. Gluhbegovic, and J.Y. Jew. Virtual Hospital. 1997. University of Iowa. WEB access: http://www.vh.org/Providers/-Textbooks/BrainAnatomy/BrainAnatomy.html.

Unité de recherche INRIA Sophia Antipolis
2004, route des Lucioles - B.P. 93 - 06902 Sophia Antipolis Cedex (France)

Unité de recherche INRIA Lorraine : Technopôle de Nancy-Brabois - Campus scientifique
615, rue du Jardin Botanique - B.P. 101 - 54602 Villers lès Nancy Cedex (France)
Unité de recherche INRIA Rennes : IRISA, Campus universitaire de Beaulieu - 35042 Rennes Cedex (France)
Unité de recherche INRIA Rhône-Alpes : 655, avenue de l'Europe - 38330 Montbonnot St Martin (France)
Unité de recherche INRIA Rocquencourt : Domaine de Voluceau - Rocquencourt - B.P. 105 - 78153 Le Chesnay Cedex (France)

Éditeur
INRIA - Domaine de Voluceau - Rocquencourt, B.P. 105 - 78153 Le Chesnay Cedex (France)
http://www.inria.fr
ISSN 0249-6399